Effects of phosphatidylcholine membrane fluidity on the conformation and aggregation of N-terminally acetylated α-synuclein

Received for publication, March 9, 2018, and in revised form, May 22, 2018 Published, Papers in Press, May 31, 2018, DOI 10.1074/jbc.RA118.002780

Emma I. O'Leary[‡], **Zhiping Jiang**[‡], **Marie-Paule Strub**[§], **and Jennifer C. Lee**[‡1]

From the [‡]*Laboratory of Protein Conformation and Dynamics and the* [§]*Biochemistry and Biophysics Center, NHLBI, National Institutes of Health, Bethesda, Maryland 20892*

Edited by Paul E. Fraser

Membrane association of α-synuclein (α-syn), a neuronal protein associated with Parkinson's disease (PD), is involved in α-syn function and pathology. Most previous studies on α-syn–membrane interactions have not used the physiologically relevant N-terminally acetylated (*N*-acetyl) α-syn form nor the most naturally abundant cellular lipid, *i.e.* phosphatidylcholine (PC). Here, we report on how PC membrane fluidity affects the conformation and aggregation propensity of N-acetyl α-syn. It is well established that upon membrane binding, α-syn adopts an α-helical structure. Using CD spectroscopy, we show that N-acetyl α-syn transitions from α-helical to disordered at the lipid melting temperature (T_m). We found that this fluidity sensing is a robust characteristic, unaffected by acyl chain length (T_m = 34–55 °C) and preserved in its homologs β- and γ-syn. Interestingly, both N-acetyl α-syn membrane binding and amyloid formation trended with lipid order (1,2-dipalmitoyl-*sn*-glycero-3-phosphocholine (DPPC) > 1,2-dioleoyl-*sn*-glycero-3-phosphocholine (DOPC)/sphingomyelin/cholesterol (2:2:1) ≥ DOPC), with gel-phase vesicles shortening aggregation kinetics and promoting fibril formation compared to fluid membranes. Furthermore, we found that acetylation enhances binding to PC micelles and small unilamellar vesicles with high curvature (r ~16–20 nm) and that DPPC binding is reduced in the presence of cholesterol. These results confirmed that the exposure of hydrocarbon chains (*i.e.* packing defects) is essential for binding to zwitterionic gel membranes. Collectively, our *in vitro* results suggest that N-acetyl α-syn localizes to highly curved, ordered membranes inside a cell. We propose that age-related changes in membrane fluidity can promote the formation of amyloid fibrils, insoluble materials associated with PD.

Parkinson's disease (PD)[2] is a chronic neurodegenerative disorder that is projected to affect up to 9 million people around the world by 2030 (1). One of the pathological hallmarks of PD is the presence of Lewy bodies, which are intracellular aggregates primarily composed of the protein α-synuclein (α-syn) (2). Mutations in *SNCA*, the gene that encodes α-syn, have also been associated with PD (3); therefore, studying the structure, function, and behavior of α-syn may provide molecular insights into the disease mechanism of PD. Although the exact physiological function of α-syn remains to be defined, previous studies have shown that it localizes to the pre-synaptic terminal of dopaminergic neurons (4) and helps regulate synaptic vesicle homeostasis and transmission (5, 6). Notably, many have described interactions between α-syn and cellular membranes as part of the pathology of PD, citing evidence of membrane disturbance and organelle dysfunction in the Golgi (7), lysosome (8), and mitochondria (9).

Substantial research over the last 20 years has been devoted to understanding the biophysics of α-syn membrane binding and structurally characterizing its membrane-bound conformations (10–13). It is well established that upon association with lipid membranes, α-syn adopts an α-helical conformation (14–16), which can be easily monitored using circular dichroism (CD) spectroscopy (17–22), a probe of secondary structure. Numerous studies have investigated membrane properties that drive α-syn binding, including vesicle curvature (23, 24), phospholipid composition (25–27), and packing defects (28, 29).

The influence of membrane fluidity on α-syn–phospholipid interactions (14, 24, 28–31) is of particular interest because PD is an age-related disease, and membranes decrease in fluidity as cells age (32). Specifically, saturated fatty acids increase in abundance during aging, whereas polyunsaturated lipids decrease (33, 34), making the membrane overall more rigid. *In vitro*, α-syn behaves as expected for anionic saturated phospholipids such as 1,2-dipalmitoyl-*sn*-glycero-3-phospho-(1′-*rac*-glycerol)) (24, 30, 31), preferring disordered lipids that exhibit both lateral and rotational movements in the fluid phase (35). Contrastingly, α-syn binding to the saturated phospholipid 1,2-

This work was supported by the Intramural Research Program at the National Institutes of Health, NHLBI. The authors declare that they have no conflicts of interest with the contents of this article. The content is solely the responsibility of the authors and does not necessarily represent the official views of the National Institutes of Health.

[1] To whom correspondence should be addressed: Laboratory of Protein Conformation and Dynamics, Biochemistry and Biophysics Center, NHLBI, National Institutes of Health, Bethesda, MD 20892. Tel.: 301-827-0723; E-mail: leej4@mail.nih.gov.

[2] The abbreviations used are: PD, Parkinson's disease; α-syn, α-synuclein; DPPG, 1,2-dipalmitoyl-*sn*-glycero-3-phospho-(1′-*rac*-glycerol); DPPC, 1,2-dipalmitoyl-*sn*-glycero-3-phosphocholine; PC, phosphatidylcholine; Chol, cholesterol; SM, sphingomyelin; *N*-acetyl, N-terminally acetylated; SUV, small unilamellar vesicle; DOPC, 1,2-dioleoyl-*sn*-glycero-3-phosphocholine; β-syn, β-synuclein; γ-syn, γ-synuclein; L/P, lipid-to-protein; 15:0 PC, 1,2-dipentadecanoyl-*sn*-glycero-3-phosphocholine; 18:0 PC (DSPC), 1,2-distearoyl-*sn*-glycero-3-phosphocholine; 12:0 lyso-PC, 1-lauroyl-2-hydroxy-*sn*-glycero-3-phosphocholine; 16:0 lyso-PC, 1-palmitoyl-2-hydroxy-*sn*-glycero-3-phosphocholine; DSC, differential scanning calorimetry; ThT, thioflavin T; TEM, transmission electron microscopy; POPC, 1-palmitoyl-2-oleoyl-*sn*-glycero-3-phosphocholine; DLS, dynamic light scattering; ITC, isothermal titration calorimetry; GUV, giant unilamellar vesicle.

dipalmitoyl-*sn*-glycero-3-phosphocholine (DPPC) is nearly abolished when the membrane is fluid (28, 30). Instead, α-syn appears to favor the ordered gel phase *in vitro* (14, 28, 29). These results for PC lipids are unusual because proteins typically do not bind to highly ordered membranes, where phospholipids have restricted motion and lipid acyl chains are fully extended, as in the case of the gel phase (35).

The close packing of lipids that occurs in the gel phase mimics the lipid ordering found in cellular lipid rafts, which are rich in cholesterol (Chol) and sphingomyelin (SM) (36, 37). Lipid rafts are proposed to be small, ordered regions found in cellular membranes that are involved in specialized functions such as trafficking and signaling (37). In the literature, there lacks a consensus whether α-syn interacts with the liquid-ordered phase found in lipid rafts, but available data (29, 31, 38–40) indicate that binding likely depends on the specific lipid compositions examined (*i.e.* choice of unsaturated phospholipid, relative amounts of SM and Chol, and the presence of anionic lipids).

It is important to note that all of the abovementioned studies used recombinant α-syn purified from *Escherichia coli*; however, N-terminal acetylation is a common post-translational modification in eukaryotes, occurring in over 80% of proteins (41). In fact, MS analysis of healthy human brains and Lewy bodies from PD patients confirmed N-terminally acetylated (N-acetyl) α-syn as the predominant form (42, 43). In yeast, a model eukaryote, N-terminal acetylation was shown to be crucial for the cellular localization of α-syn. Upon knockdown of *N*-acetyltransferase B, α-syn was observed to redistribute from the plasma membrane to the cytosol (44). Furthermore, the N terminus of α-syn is generally recognized as the membrane-binding region (12). In fact, the first 15 residues nearly recapitulated the binding properties of the full-length protein (20), suggesting that the N terminus serves as a membrane anchor. Therefore, N-terminal acetylation is anticipated to impact α-syn lipid binding. Indeed, NMR studies showed that N-acetyl α-syn exhibited stronger membrane binding than unacetylated α-syn (45, 46). However, others have reported no effect (47).

The aim of our work is to understand the molecular basis of N-acetyl α-syn interactions with physiologically-relevant cellular membranes. Toward this goal, we carried out a detailed *in vitro* study monitoring the conformational change of N-acetyl α-syn upon binding to gel and liquid-ordered phases, two areas where less attention has been given in the literature. Specifically, we sought to evaluate secondary structural changes of N-acetyl α-syn in the presence of PC lipids (Fig. 1). It is essential to study PC lipids because they are the most common lipid type found in animal cells. Furthermore, the literature on α-syn interactions with zwitterionic membranes currently lags far behind that of anionic lipids, in part due to their weak binding to α-syn compared with anionic phospholipids. Here, we used small unilamellar vesicles (SUVs) and CD spectroscopy to systematically probe the effects of PC lipid acyl chain length, temperature (*i.e.* membrane fluidity), Chol (*i.e.* packing defects), and membrane curvature on the α-helicity of N-acetyl α-syn. Finally, the aggregation propensity of N-acetyl α-syn was investigated in the presence of biologically-relevant lipid raft mixtures and compared with fluid-phase 1,2-dioleoyl-*sn*-glycero-3-phosphocholine (DOPC) and gel-phase DPPC membranes to probe the complex relationship surrounding lipid order, α-helical conformation, and amyloid formation kinetics.

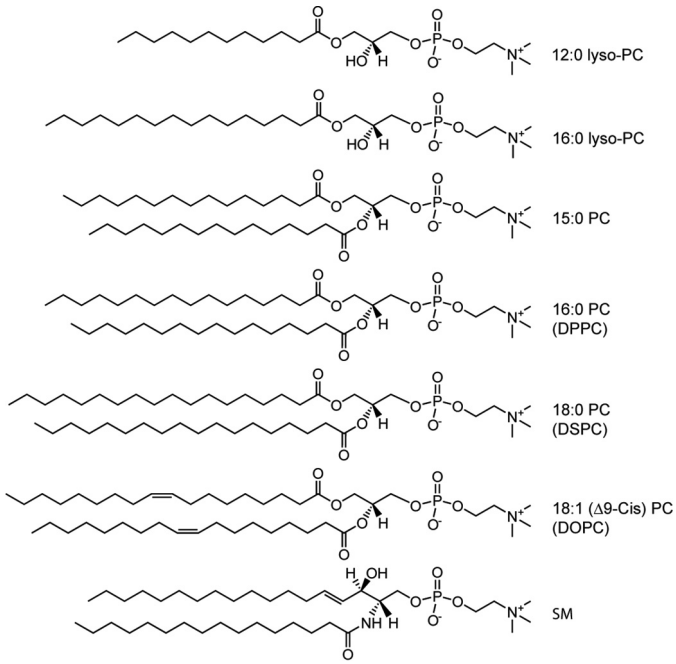

Figure 1. Chemical structures of phospholipids used in this study.

Results

DPPC fluidity sensing by α-, β-, and γ-syn

Previous studies have shown that α-syn binds with greater α-helical content to saturated PC SUVs in the gel phase compared to the fluid phase (28, 29). It is unknown, however, whether this behavior is preserved for the two other naturally-occurring human synuclein homologs, β-syn and γ-syn. In particular, we are interested in membrane binding that is coupled to the promotion of α-helical polypeptide conformation. Here, we rely on CD spectroscopy to capture the secondary structural changes of the protein in response to membrane fluidity.

First, we repeated the CD spectroscopic experiments by Nuscher *et al.* (28). In accordance with previous results, α-syn transitioned from disordered–to–α-helical as DPPC SUVs were added, as seen by the appearance of double-negative peaks at 208 and 222 nm (Fig. 2*A*, *inset*). The observed α-helical content was stronger at 20 °C (gel) compared to 50 °C (fluid) (Fig. 2*A*). These results indicate stronger membrane association based on the enhancement of α-helical content. To corroborate this assertion, we used an orthogonal method, isothermal calorimetry, to confirm that binding measured by the release of heat was greater at 20 °C and negligible at 50 °C (Fig. S1), consistent with results by Nuscher *et al.* (28).

Importantly, the conformation of α-syn ($[\Theta]_{222\ nm}$) exhibited exquisite sensitivity to the transition melting temperature of DPPC ($T_m = 39$ °C), remaining α-helical at $T < T_m$ and unfolding beyond T_m (Fig. 2*B*). This gel-phase preference was maintained over a wide range of lipid-to-protein (L/P) molar ratios

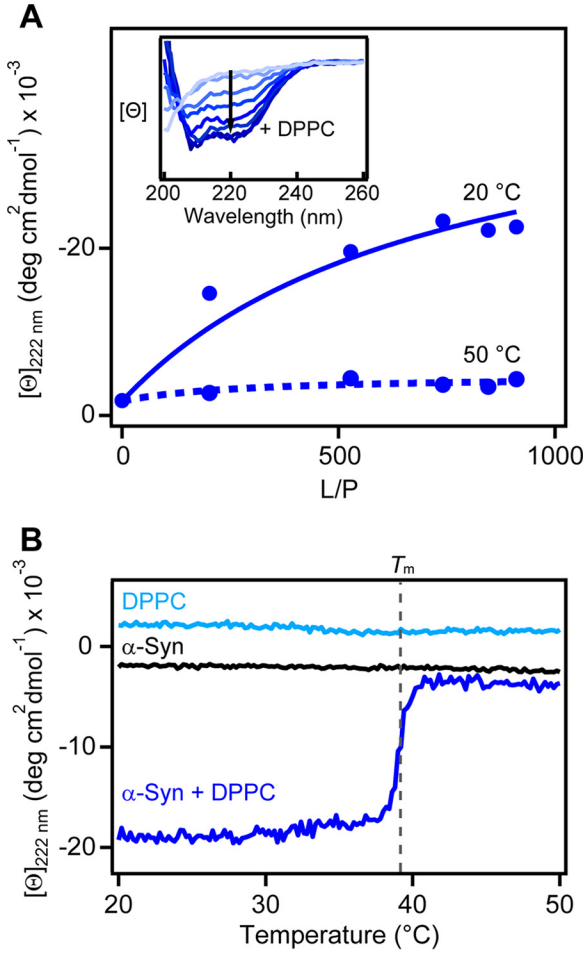

Figure 2. Secondary structural changes of α-syn upon binding to DPPC vesicles in the gel (20 °C) and fluid (50 °C) phases probed by CD spectroscopy. *A,* binding curves from mean residue ellipticity ($[\theta]_{222\ nm}$) at 20 *versus* 50 °C. Fits to a two-state equilibrium are shown as *solid* and *dashed lines* (K_p = 700 ± 200 and 100 ± 200 M^{-1} for 20 and 50 °C, respectively). *Inset*, representative CD spectra of α-syn (5 μM) as a function of increasing vesicles (0–3.2 mM DPPC, shown as *light-to-dark blue traces*) at 20 °C. *B,* effect of increasing temperatures on the α-helical content ($[\theta]_{222\ nm}$) of α-syn in the presence of DPPC vesicles (*dark blue,* L/P = 640). *Gray dashed line* indicates the gel-to-fluid–phase transition temperature of DPPC (T_m = 39 °C) as determined by DSC. Lipid (*light blue,* [DPPC] = 3.2 mM) and protein (*black*, [α-syn] = 5 μM) alone controls are also shown. Scan rate = +20 °C/h.

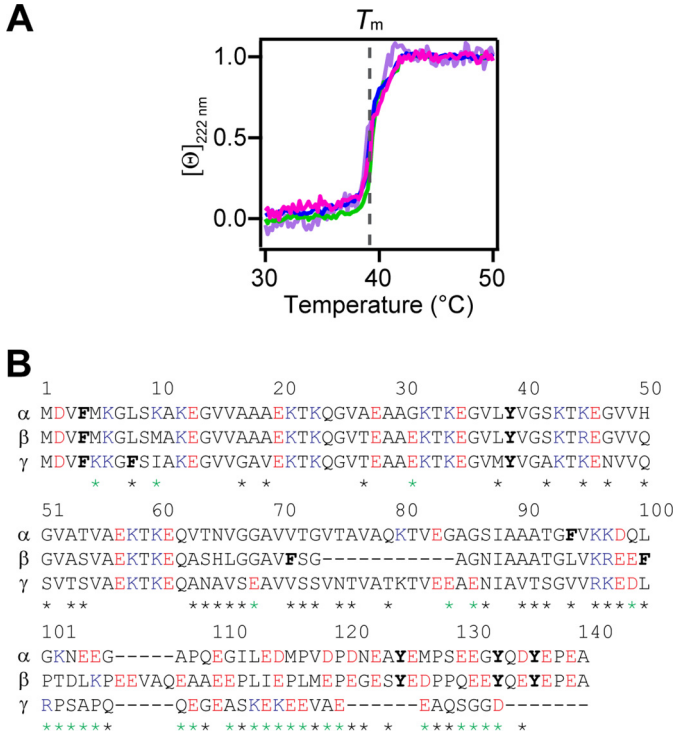

Figure 3. DPPC fluidity sensing by synuclein variants. *A,* fluidity sensing by N-acetyl α-syn (*magenta*), α-syn (*green*), β-syn (*blue*), and γ-syn (*purple*) as determined by changes in $[\theta]_{222\ nm}$ in the presence of DPPC vesicles (L/P = 640–890, [protein] = 5 μM). Data were normalized for the ease of comparison. *Gray dashed line* indicates the T_m of DPPC. Scan rate = +20 °C/h. *B,* amino acid sequence alignments of the human synuclein family. Basic, acidic, and aromatic residues are marked as *blue, red*, and *bold*, respectively. Sequence differences are denoted with a *green* or *black asterisk* when the charge was changed or conserved, respectively. The program ALIGN was used (https://www.uniprot.org/align) (Please note that the JBC is not responsible for the long-term archiving and maintenance of this site or any other third party hosted site).

(Fig. S2). Interestingly, the ability to sense DPPC membrane fluidity was conserved across the human synuclein family; both β-syn and γ-syn transitioned from α-helical to disordered around the T_m (Fig. 3*A*). Temperature scans were performed at a L/P ratio near saturation based on CD titration curves (Fig. S3). Compared with α-syn, β-syn lacks 11 residues in the central region, and γ-syn has a shortened C-terminal tail (Fig. 3*B*), indicating that neither of these regions are responsible for fluidity sensing. Instead, membrane fluidity sensing is likely dominated by the N-terminal portion, where the sequences are nearly identical in the first 44 residues (95.5 and 84% for β- and γ-syn, respectively).

Finally, the effect of N-terminal acetylation was examined. The promotion of α-helicity and fluidity sensing by N-acetyl α-syn were indistinguishable from that of unacetylated α-syn (Figs. 3*A* and Fig. S3). Therefore, N-terminal acetylation does not seem to play a significant role in fluidity sensing.

Effect of membrane thickness on fluidity sensing by N-acetyl α-syn

Because biological membranes are complex and have different membrane thicknesses, we investigated whether fluidity sensing by N-acetyl α-syn extends to zwitterionic membranes with varying acyl chain lengths: 15:0 PC (1,2-dipentadecanoyl-*sn*-glycero-3-phosphocholine), 16:0 PC (DPPC), and 18:0 PC (1,2-distearoyl-*sn*-glycero-3-phosphocholine (DSPC)), although we expected little effect as α-syn inserts shallowly into the outer leaflet of the bilayer (18, 20, 48). In accord, minor differences in α-helicity were found in response to 15:0, 16:0, and 18:0 PC vesicles in the gel phase for both unacetylated and N-acetyl α-syn (Fig. S4). We note that these similarities solely reflect gross α-helical content and do not exclude the existence of affinity differences and/or unstructured proteins bound to the membrane.

Nevertheless, N-acetyl α-syn detected changes in membrane fluidity via the loss of α-helicity at or before the T_m (Fig. 4) for all three lipids, despite the T_m varying from 34 to 55 °C (Fig. S5). Our data suggest that despite the protein residing on the periphery of the vesicle, α-syn can respond to lipid rearrangements that occur during the gel-to-fluid phase transition.

Interestingly, when comparing CD titrations of 15:0 PC vesicles with high curvature (r = 19.7 nm), N-acetyl α-syn exhibited a noticeably enhanced CD signal compared to the unacety-

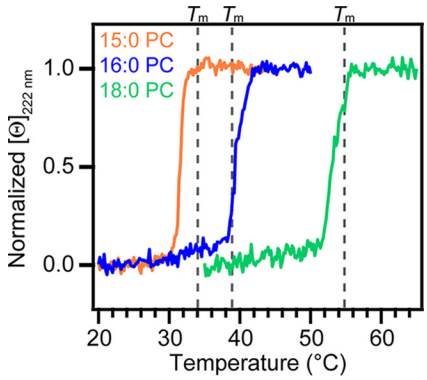

Figure 4. Effect of lipid acyl chain length on fluidity sensing by N-acetyl α-syn. Changes in $[\theta]_{222\ nm}$ of N-acetyl α-syn (5 μM) in the presence of 15:0 PC (*orange*, L/P = 370), 16:0 PC (*blue*, L/P = 510), and 18:0 PC (*green*, L/P = 410) vesicles are shown. *Gray dashed lines* mark the melting temperatures of 15:0 PC (T_m = 34 °C), 16:0 PC (T_m = 39 °C), and 18:0 PC (T_m = 55 °C), respectively, as determined by DSC. Data were normalized for the ease of comparison. Scan rate = +20 °C/h.

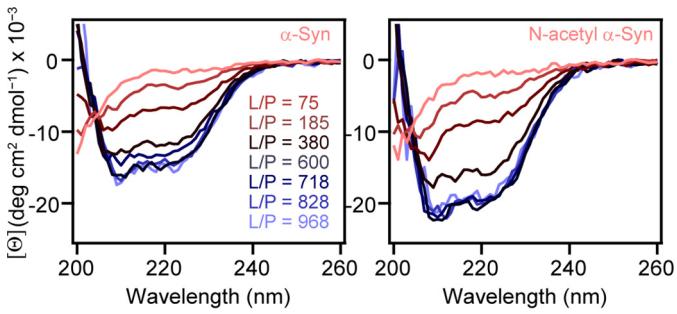

Figure 5. Impact of N-terminal acetylation on the secondary structure of α-syn in the presence of 15:0 PC vesicles. CD spectra of α-syn (*left*) and N-acetyl α-syn (*right*) as a function of increasing vesicles ([15:0 PC] = 0–4.8 mM, [protein] = 5 μM) at 20 °C are shown as *red*-to-*blue traces*. Average hydrodynamic radius was 19.7 nm by DLS.

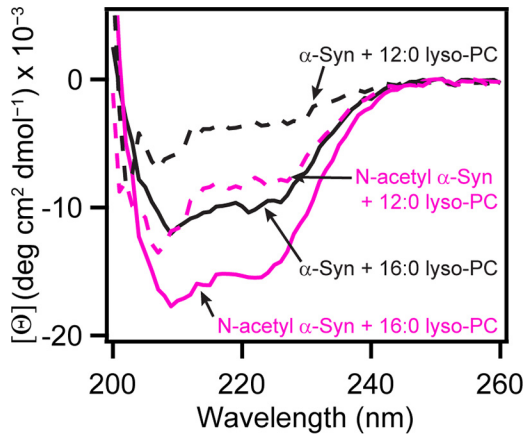

Figure 6. CD comparison of α-syn and N-acetyl α-syn in the presence of zwitterionic micelles. Representative CD spectra of α-syn (*black*) and N-acetyl α-syn (*magenta*) in the presence of 12:0 lyso-PC (*dotted trace*) and 16:0 lyso-PC (*solid trace*) micelles ([lyso-PC] = 25 mM and [protein] = 5 μM) at 20 °C are shown.

lated form (Fig. 5), suggesting that the effect of N-terminal acetylation on vesicle association is curvature-dependent.

Effect of N-terminal acetylation on α-syn binding to PC micelles

To further probe the importance of membrane curvature on N-acetyl α-syn binding, we compared the binding of unacetylated and N-acetyl α-syn using two zwitterionic micelles with varying chain lengths: 12:0 lyso-PC (1-lauroyl-2-hydroxy-*sn*-glycero-3-phosphocholine) and 16:0 lyso-PC (1-palmitoyl-2-hydoxy-*sn*-glycero-3-phosphocholine). Micelles were made at concentrations (25 mM) significantly higher than the critical micelle concentrations (49) of the lysolipids to ensure that there was an excess number of micelles. Consistent with our highly curved 15:0 PC vesicle data, greater α-helicity by the N-acetyl form of α-syn was observed for the lyso-PC micelles (Fig. 6). Additionally, α-helical formation by unacetylated and N-acetyl α-syn was increased for 16:0 lyso-PC micelles compared with 12:0 lyso-PC (Fig. 6), suggesting that α-helical structure stabilization is influenced by lipid acyl chain length. Taken together, our data suggest that N-terminal acetylation promotes the formation of α-helical structure in the presence of membranes with high curvature.

Effect of cholesterol on DPPC binding and fluidity sensing by N-acetyl α-syn

Packing defects are defined as areas in the membrane where hydrophobic acyl chains are solvent-exposed due to the geometrical misalignment of phospholipids in a spherical vesicle (50). Packing defects underlie one of the major mechanisms proposed for α-syn binding to both gel and fluid phases. In addition, it has been well documented that packing defects increase in number as the radius of a vesicle decreases (50, 51).

To test this mechanism, we added increasing amounts of Chol to DPPC to block defects in the membrane. Equilibrium binding curves revealed that small quantities of Chol (5, 10, and 20%, Fig. 7*A*) weakened the binding of N-acetyl α-syn to DPPC vesicles, whereas larger amounts of Chol (30%) abolished it (Fig. S6), supporting the packing defect binding mechanism. A similar effect of Chol on binding behavior was also measured for unacetylated α-syn (Fig. S6).

Furthermore, DPPC fluidity sensing by N-acetyl α-syn was preserved when 5 or 10% Chol was present (Fig. 7*B*). By differential scanning calorimetry (DSC), the T_m of DPPC shifted from 39 to 41 °C upon the addition of Chol (Fig. S7), and instead of N-acetyl α-syn sensing the main lipid transition at 41 °C, it began changing conformation from α-helical to disordered at $T \sim 38$ °C (Fig. 7*B*). This earlier transition measured by CD corresponds to a minor peak to the left of the main transition on the DSC thermogram (Fig. S7). This minor peak became more prominent as more Chol was added, and we interpret this to be the ripple phase. The ripple phase, also called the pretransition, occurs between the transition from the gel phase to the fluid phase (35). Therefore, N-acetyl α-syn seems to become sensitive to the ripple phase as Chol is added to DPPC SUVs.

N-Acetyl α-syn binding to zwitterionic liquid-ordered phase vesicles

Next, the conformational change of N-acetyl α-syn was studied using a more physiologically-relevant lipid composition. We chose to model the liquid-ordered phase found in lipid rafts by mixing DOPC, SM, and Chol in a 2:2:1 ratio, respectively (52). We observed direct evidence that N-acetyl α-syn interacts

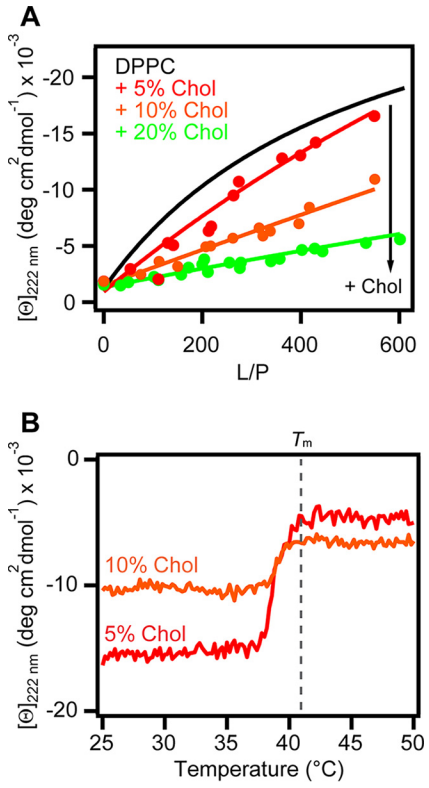

Figure 7. Concentration dependence of cholesterol on the binding of N-acetyl α-syn to DPPC vesicles. *A,* equilibrium binding curves from $[\theta]_{222\ nm}$ for N-acetyl α-syn (5 μM) binding to DPPC (*black,* global fit) and DPPC with 5% (*red*, $n = 2$), 10% (*orange*, $n = 2$), and 20% (*green*, $n = 3$) cholesterol (Chol) at 20 °C. Global fits to a two-state equilibrium are shown as solid lines, and K_p values were 400 ± 200, 200 ± 100, and 80 ± 60 M^{-1} for 5, 10, and 20% Chol, respectively. *B,* effect of increasing temperatures on N-acetyl α-syn $[\theta]_{222\ nm}$ in the presence of DPPC + 5% (*red*, L/P = 456) and 10% Chol (*orange,* L/P = 501). Scan rate = +20 °C/h.

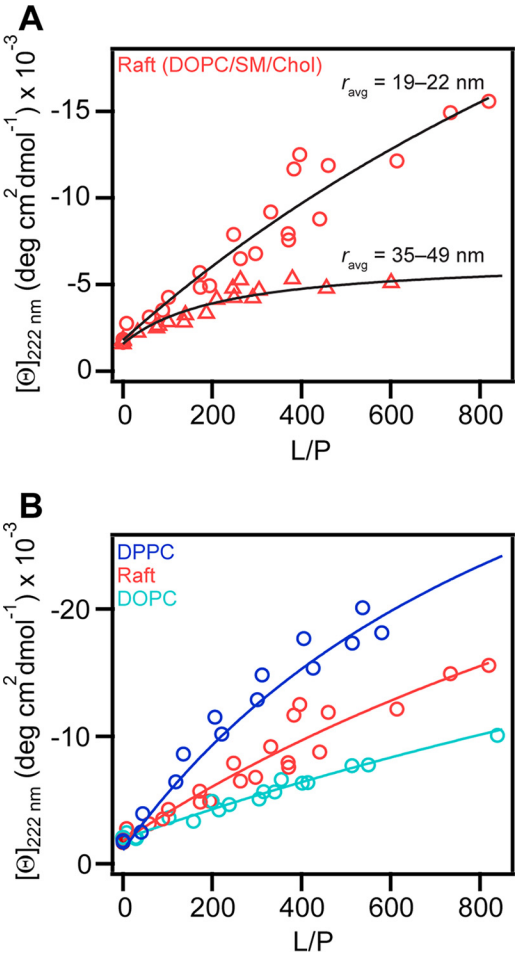

Figure 8. Binding of N-acetyl α-syn to the liquid-ordered phase as determined by CD spectroscopy. *A,* effect of vesicle size on N-acetyl α-syn (5 μM) binding to DOPC/SM/Chol (2:2:1) vesicles. Average hydrodynamic radius ranged from either 19 to 22 nm (*circles*, $n = 2$) or 35 to 49 nm (*triangles*, $n = 2$). Data were fit to a two-state equilibrium shown as *black solid lines*, and K_p values were 300 ± 100 and 1500 ± 500 M^{-1} for small and large vesicles, respectively. *B,* equilibrium binding curves generated at 20 °C from $[\theta]_{222\ nm}$ for N-acetyl α-syn (5 μM) to DOPC (*teal*, $n = 3$) and DPPC (*dark blue*, $n = 2$). For ease of comparison, the data for DOPC/SM/Chol (2:2:1) (*pink*, $n = 2$) from *panel A* are shown again. Global fits to a two-state equilibrium are shown as *solid lines*, and K_p values were 100 ± 100, 300 ± 100, and 700 ± 200 M^{-1} for DOPC, DOPC/SM/Chol (2:2:1), and DPPC, respectively.

with DOPC/SM/Chol vesicles in a curvature-dependent manner (Figs. 8*A* and Fig. S8), where greater helical content is observed in the presence of vesicles with smaller average hydrodynamic radii. In addition, compared to the unacetylated form, N-terminal acetylation enhanced the α-helical content of α-syn in the presence of lipid raft SUVs with high curvature ($r = 16$ nm) (Fig. S9), consistent with our previous observations for 15:0 PC SUVs (Fig. 5) and lyso-PC micelles (Fig. 6). However, unlike what we presented earlier for DPPC (Figs. 3*B* and 4), N-acetyl α-syn remained α-helical in the presence of DOPC/SM/Chol from 25 to 50 °C (Fig. S10), indicating that it is stably bound at physiological temperatures.

As both fluid and liquid-ordered phases coexist in DOPC/SM/Chol vesicles (52), we used CD to measure secondary structural changes of N-acetyl α-syn upon binding to DOPC ($T_m = -17$ °C) and compared it with DPPC ($T_m = 39$ °C) to determine whether N-acetyl α-syn is bound to the fluid- or liquid-ordered phase. We found that the α-helicity of N-acetyl α-syn is decreased with fluid DOPC compared to gel DPPC vesicles (Fig. 8*B*). Because binding to DOPC/SM/Chol was in between that of DOPC and DPPC, we infer that N-acetyl α-syn is bound to the liquid-ordered phase in the lipid raft mixture with the underlying assumption that α-syn must be lipid-bound to adopt an α-helical conformation.

N-Acetyl α-syn amyloid formation in the presence of gel-, fluid-, and liquid-ordered vesicles

To determine whether membrane fluidity influences N-acetyl α-syn amyloid formation, monomers were mixed with either gel-phase DPPC, lipid raft mixture DOPC/SM/Chol, or fluid-phase DOPC SUVs and monitored over time at 37 °C using thioflavin T (ThT) (Fig. 9*A*), which increases in fluorescence intensity in the presence of amyloid fibrils. Typical aggregation kinetics follow a sigmoidal trend: an initial lag phase, followed by a rapid intensity increase known as the growth phase, and a stationary phase. Transmission EM (TEM) and CD were obtained before (Fig. S11) and after aggregation to visualize fibril morphology (Figs. 9*B* and Fig. S12) and detect β-sheet structure associated with amyloid formation (Fig. 9*C*), respectively.

After 63 h, amyloid fibrils were present in all samples; however, the kinetics and total β-sheet content were lipid compo-

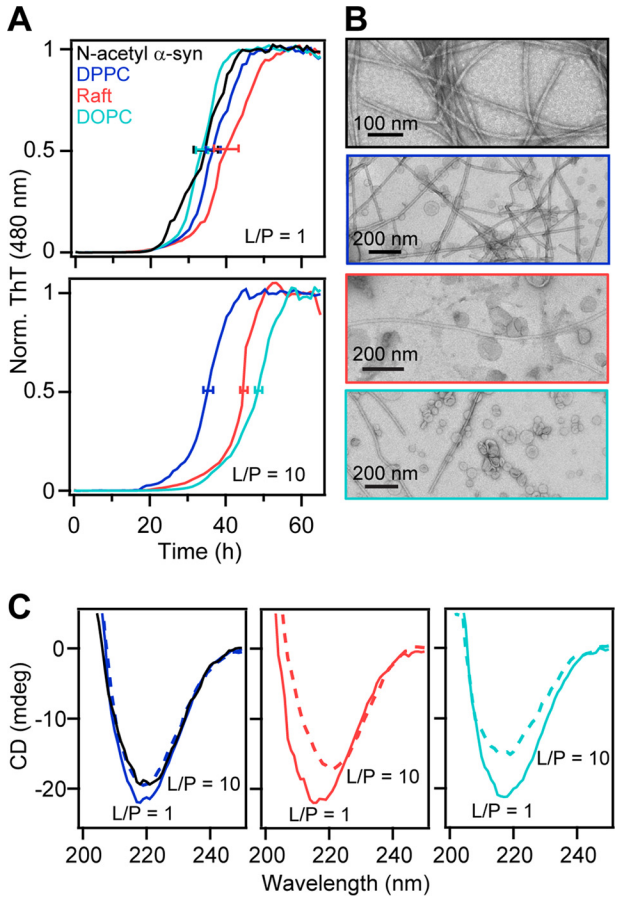

Figure 9. Aggregation kinetics of N-acetyl α-syn in the presence of gel, liquid-ordered, and fluid-phase zwitterionic vesicles. *A,* amyloid formation of N-acetyl α-syn (50 μM) at 37 °C with shaking monitored by ThT fluorescence (10 μM) at pH 7 (20 mM MOPS, 100 mM NaCl) in the absence (*black*) or presence of DPPC (*blue*), DOPC/SM/Chol (2:2:1) (*pink*), and DOPC (*teal*) vesicles at L/P = 1 (*top*) and L/P = 10 (*bottom*). ThT data were normalized and averaged ($n \geq 2$). *Error bars* denote mean $t_{1/2} \pm$ S.D. (protein alone = 34 ± 6 h; DPPC = 38 ± 4 (L/P = 1) and 36 ± 2 h (L/P = 10); raft = 41 ± 6 (L/P = 1) and 45 ± 0.6 h (L/P = 10), DOPC = 34 ± 3 (L/P = 1), and 48 ± 0.6 h (L/P = 10)). *B,* representative TEM images of N-acetyl α-syn fibrils formed in the absence (*black*) or presence of DOPC, DPPC, and DOPC/SM/Chol (2:2:1) vesicles (L/P = 10). Lipid compositions are colored as in *A*. *Scale bars* are as indicated. *C,* CD spectra at 20 °C of post-aggregation samples at L/P = 1 (*solid traces*) and L/P = 10 (*dotted traces*). Protein alone (*black*) is also shown in the *left panel* for comparison. Lipid compositions are colored as in *A*.

sition- and concentration-dependent. When stoichiometric amounts of lipids were present (L/P = 1), little or no effect on aggregation kinetics was observed for all samples compared with the protein alone (Fig. 9*A*, *top panel*). Similar lag and growth phases were observed, and $t_{1/2}$ (time required to reach half the maximum ThT intensity) values were within one standard deviation of the protein in buffer (34 ± 6 h). However, as the amount of vesicles increased (L/P = 10), both DOPC/SM/Chol and DOPC suppressed amyloid formation ($t_{1/2}$ = 45 ± 0.6 and 48 ± 0.6 h, respectively, see Fig. 9*A*, *bottom panel*). In contrast, DPPC had a minimal effect on the aggregation kinetics, where $t_{1/2}$ remained similar (36 ± 2 h) to the protein alone (34 ± 6 h) at L/P = 1 (38 ± 4 h). We note that while the absolute $t_{1/2}$ varied from plate to plate, the relative trends were consistent and reproducible (n = 7 plates, see Fig. S13 for another data set).

Significantly less amyloid fibrils were formed at L/P = 10 as indicated by the presence of higher levels of soluble protein after aggregation (Fig. S14). This was also corroborated by CD, in which lower absorption was observed for L/P = 10 compared with L/P = 1 at 218 nm, characteristic of β-sheet content (Fig. 9*C*). Interestingly, there were noticeable differences in the β-sheet content among the lipid compositions at L/P = 10; DPPC had the highest β-sheet content, followed by the raft and DOPC, providing further evidence that amyloid formation is supported the strongest by gel-phase DPPC (Fig. 9*C*). These CD trends were also confirmed using samples aggregated in the absence of ThT (Fig. S15). In addition, we checked whether amyloid formation can occur at a much higher lipid concentration (L/P = 100). For all three lipid compositions, amyloid fibrils were visualized by TEM (Fig. S16), which contrasts with previous work that showed complete inhibition of α-syn aggregation by POPC (1-palmitoyl-2-oleoyl-*sn*-glycero-3-phosphocholine) (17). Collectively, our results indicate that N-acetyl α-syn aggregation is modulated by the fluidity of the membrane, preferring more ordered vesicles as a surface for amyloid formation compared with fluid membranes.

Discussion

Focusing on the effect of lipid order, we performed a series of *in vitro* experiments exploring the impact of PC phospholipids and zwitterionic lipid raft mixtures on N-acetyl α-syn conformation and aggregation. First, we studied membrane fluidity sensing from the perspective of the protein, monitoring the loss of α-helicity as the lipid phase transitioned from gel-to-fluid. All three members of the synuclein family (α-, β-, and γ-syn) transitioned around the T_m of DPPC as observed by CD (Fig. 3*A*). Therefore, we propose that the highly homologous N-terminal amphipathic region is a major determinant of this shared behavior. However, because α-helicity is a global measure, it is unknown to what extent structural heterogeneity and subpopulations exist, and further study using high resolution methods are needed to address this question.

Because the greatest sequence similarity among the homologs is found in the first 44 residues, we expected that N-terminal acetylation of α-syn would enhance binding, which others have reported using CD and NMR with anionic vesicles (45, 46). Here, we observed that N-terminal acetylation increased the α-helical content of α-syn in the presence of lyso-PC micelles (Fig. 6) and PC SUVs with high curvature ($r \sim$16–20 nm) (Figs. 5 and 8*A*). From a biological perspective, preferential binding to small vesicles could help N-acetyl α-syn localize to synaptic vesicles ($r \sim$20 nm) over other flat membrane surfaces inside a cell.

The observed increase in α-helical signal for 16:0 lyso-PC compared with 12:0 lyso-PC (Fig. 5) could indicate that N-acetyl α-syn has an acyl chain length preference. However, because N-acetyl α-syn only inserts into the outer leaflet of the bilayer (18, 20, 48), as seen by similar binding to vesicles composed of different PC acyl chain lengths (Fig. S5), perhaps its sensitivity is related to differences in the specific lipid-bound conformation (13). α-Syn has been shown to adopt different structures as a function of membrane curvature: a bent helix on micelles (53) *versus* an extended α-helix on vesicles (48). Thus,

the increase in α-helicity may indicate that a longer helix can be accommodated on a slighter larger PC micelle.

Interestingly, fluidity sensing by N-acetyl α-syn was preserved across different PC acyl chain lengths (Fig. 4), which was remarkable because the T_m of the lipids ranged from 34 to 55 °C (Fig. S4). Thus, fluidity sensing is a robust characteristic of N-acetyl α-syn that is not affected by bilayer thickness or elevated temperatures. Although DPPC bilayers have been shown to thicken by ~0.6 nm during its phase transition from fluid to gel (54), our results suggest that preferential binding by N-acetyl α-syn to the gel phase is not likely driven by membrane thickness.

Instead, the observed Chol-dependent binding of N-acetyl α-syn to DPPC (Fig. 7*A*) reaffirms that packing defects play a pivotal role in the membrane-binding mechanism. Our explanation is consistent with previous findings that described α-syn binding as an exothermic process that "heals" packing defects (28), alleviating the energetic cost of leaving the hydrophobic acyl chains unprotected. Packing defects are particularly important for binding to zwitterionic lipids due to the absence of strong electrostatics, which dominate for anionic lipids (15, 25–27, 39).

Packing defects also have implications for the biological function of α-syn. For example, defects increase stress on the lipid bilayer, priming the membrane for fusion (55). This agrees with current evidence that α-syn helps synaptic transmission by interacting with the SNARE complex during exocytosis (56–58). Moreover, cellular localization of α-syn to synaptic terminals has been attributed to lipid rafts with liquid-ordered domains (59).

Despite studies reporting α-syn binding to the liquid-ordered phase, there is little consensus, particularly for zwitterionic lipid raft mixtures, whether α-syn can interact (29, 31, 38, 39). Here, we present definitive CD data that show N-acetyl α-syn binds with an α-helical conformation to DOPC/SM/Chol in a curvature-dependent manner (Fig. 8*A*). Therefore, it is unsurprising that little to no binding was seen in prior work using large or giant unilamellar vesicles (GUVs) to model zwitterionic lipid rafts (31, 39).

One advantage, however, of using GUVs is the ability to visualize phase separation and domain formation using fluorescence microscopy (31), which is not possible for SUVs. But, according to phase diagrams, a 2:2:1 mixture of DOPC/SM/Chol results in the co-existence of fluid and liquid-ordered phases (52). Because the α-helical content observed in the presence of DOPC/SM/Chol was greater than that of fluid DOPC but less than gel DPPC, we infer that the raft mixture had characteristics in between that of gel and fluid membranes. Furthermore, because α-helical formation in the presence of DOPC/SM/Chol (Fig. 8*B*) was enhanced compared with DPPC/Chol containing the same proportion of Chol (20%, Fig. 7*A*), which serves as a mimic for the liquid-ordered region of SM/Chol, we hypothesize that N-acetyl α-syn would bind more favorably to the interfacial regions rather than the Chol-enriched domains. This proposal is reasonable as packing defects are likely abundant at the interface between fluid and liquid-ordered phases.

Based on ThT fluorescence, CD spectroscopy, and TEM (Fig. 9), we conclude that N-acetyl α-syn aggregation also trends with membrane fluidity. When the level of free α-syn is high, like in the disease state, amyloid formation is observed (L/P = 1). However, as more lipid vesicles are added (L/P = 10), aggregation is suppressed, especially by DOPC/SM/Chol and DOPC (Fig. 9). This suppression is enhanced further at L/P = 50 and 100 (data not shown), where nearly all the proteins are lipid-bound. This difference in aggregation propensity based on relative protein and lipid concentrations highlights an important link between lipid-to-protein stoichiometry and the health of a cell.

The experimental conditions are disease-relevant because an abundance of α-syn is genetically associated with PD in familial cases of *SNCA* (α-syn) gene duplication and triplication (60, 61). Furthermore, elevated levels of α-syn mRNA have been documented in PD patients (62), and α-syn protein levels are recognized to play a role in its cytotoxic potential (63).

Amyloid fibril formation was supported the strongest by DPPC, followed by DOPC/SM/Chol and DOPC. This trend was unanticipated as one might have expected that fluid membranes would better facilitate protein conformational dynamics and promote interprotein encounters on the vesicle through increased lipid mobility. On the other hand, perhaps stronger binding to DPPC could lead to more recruitment and accumulation of proteins on the membrane, promoting protein–protein interactions on a two-dimensional surface. The immobilized proteins could then serve as interaction sites for free monomers to initiate aggregation, thereby enhancing primary nucleation. These results suggest that lipid rafts and other ordered regions found in biological membranes could serve as locations for enriched amyloid formation as opposed to fluid membranes. Interestingly, membrane fluidity also has been shown to influence α-syn aggregation for anionic phospholipids, in which different stimulation effects were seen for saturated *versus* unsaturated lipid membranes (64).

Amyloid formation in the presence of DOPC vesicles (Fig. S16) was also surprising because strong inhibition by POPC vesicles was previously observed (17). However, molecular simulations report a higher number of packing defects for DOPC compared with POPC due to the additional double bond (50), suggesting that the presence of membrane defects (*i.e.* enhanced protein association) could be related to aggregation propensity. Although speculative, this hypothesis is similar to that offered by others who favor protein crowding on the membrane surface as a mechanism (64). Additional work on detecting oligomeric forms and characterizing their specific intermolecular contacts facilitated by distinct phospholipid compositions is needed to support these proposals.

In conclusion, our work provides evidence that membrane fluidity is directly related to the propensity of N-acetyl α-syn to bind zwitterionic membranes and form amyloid fibrils. We suggest that fluid lipid membranes play a key role in α-syn homeostasis by preventing the protein from aggregating. However, depending on the lipid composition (*e.g.* saturated lipids and Chol) as well as lipid-to-protein levels, the balance can be perturbed and hence a disease risk factor. Consistent with our assertion, PD patients were observed to have increased levels of saturated lipids in the frontal cortex compared with controls (33), and cell culture experiments showed that membranes

become more rigid as they age due to increases in Chol (32–34). Taken together, our results suggest that changes in membrane fluidity can alter the equilibrium of free *versus* membrane bound α-syn, and therefore impact the aggregation of α-syn into amyloid fibrils, insoluble materials associated with neurodegeneration.

Experimental procedures

Materials

ThT, sodium chloride (≥99.5%), L-ascorbic acid (≥99%), hydrogen peroxide (≥30%), ammonium molybdate (≥99.98%), MOPS (≥99.5%), SDS (≥99%), and sodium phosphate dibasic standard (1000 ± 4 mg/liter) were purchased from Sigma. All lipids (DPPC (16:0 PC), 1-lauroyl-2-hydroxy-*sn*-glycero-3-phosphocholine (12:0 lyso-PC), 1-palmitoyl-2-hydroxy-*sn*-glycero-3-phosphocholine (16:0 lyso-PC), 1,2-dipentadecanoyl-*sn*-glycero-3-phosphocholine (15:0 PC), DSPC (18:0 PC), DOPC, and egg SM) and ovine Chol were purchased from Avanti Polar Lipids (Alabaster, AL). All materials were used as received.

Protein expression and purification

The cDNAs corresponding to β-syn and γ-syn were obtained from GenScript (Piscataway, NJ). Both were subcloned into a pET-22b vector (Novagen-EMD Millipore) using NdeI and BamHI restriction sites with primers (Eurofins MWG Operon) encoding the initiation codon (GGA ATT CCA TAT GGA CGT GTT CAT GAA GGG C and GGA ATT CCA TAT GGA TGT CTT CAA GAA GGG C for β- and γ-syn, respectively) and primers containing an opal stop codon (GTA TGA GCC AGA GGC GTA GGA TCC GCG and CCA GAG TGG GGG AGA CTA GGA TCC GCG, for β- and γ-syn, respectively). The entire coding regions of the proteins were sequenced (Macrogen USA) to confirm the constructs.

Recombinant human α-, β-, and γ-syn were expressed and purified according to previous methods (21). α-, β-, and γ-syn eluted in the ranges of ~210–260, ~230–310, and ~130–140 mM NaCl, respectively, on a Mono Q column (16/10, Amersham Biosciences). Protein concentrations for α-syn and β-syn were determined using a molar extinction coefficient ($\epsilon_{280\ nm}$ = 5120 M^{-1} cm^{-1}) estimated based on amino acid content and a spectrophotometer (Cary 300 Bio). Because of the small molar extinction coefficient for γ-syn ($\epsilon_{280\ nm}$ = 1280 M^{-1} cm^{-1}), protein concentrations were determined using the Micro BCA Protein Assay (ThermoFisher Scientific, Waltham, MA) and a microplate reader (Tecan Infinite M200 Pro).

N-Acetyl α-syn was expressed by modifying our previous method (65). The plasmids pRK172 (66) and pNatB (67) were co-transformed into One Shot BL21(DE3) cells (Invitrogen) under the selective pressure of carbenicillin (100 μg/ml) and chloramphenicol (35 μg/ml). Overnight starter cultures (25 ml) were grown in LB media at 37 °C with shaking and used to inoculate 1 liter of TB media supplemented with 0.4% glycerol. Upon reaching an $OD_{600\ nm}$ of ~0.5, the temperature was reduced to 30 °C, and the cells were induced with 1 mM isopropyl 1-thio-β-D-galactopyranoside for ~15 h. The purification protocol of N-acetyl α-syn was similar to previous protocols for α-syn (65) but with additional steps of three freeze-thaw cycles (dry ice and 37 °C water bath) and probe-tip sonication on ice (Branson 450, output 4, 50% duty cycle, 4 min) to improve lysis efficiency. N-acetyl α-syn eluted in the range of ~210–230 mM NaCl on a Mono Q column (16/10, Amersham Biosciences).

Sample homogeneity and identity were evaluated for all proteins using LC-MS and SDS-PAGE visualized by silver staining (Pharmacia PhastGel 8–25%). Based on MS, α-syn was 100% acetylated with a small population (4%) of methionine-oxidized species. All purified proteins were flash-frozen in liquid nitrogen and stored at −80 °C until use.

Lipid vesicle preparation

SUVs were prepared according to prior procedures (17) with minor modifications. Lipids (~8 mM) dissolved in chloroform were dried under flowing nitrogen gas and stored in a vacuum oven (40 °C, <20 kPa) overnight. Lipid films were rehydrated in buffer (20 mM MOPS, 100 mM NaCl, pH 7) and resuspended using bath sonication (Branson 2510 Ultrasonic Cleaner). To make SUVs, lipid solutions were probe-tip–sonicated for 45 min in a water bath (Branson 450, output 6, 50% duty cycle). Water baths were set at a temperature above the transition melting temperature of the lipid. Vesicles were centrifuged (17,000 × *g*, 20 min, room temperature) and syringe-filtered through a 0.22-μm membrane to remove particulates.

Micelle stocks (200 mM) were produced by hydrating 12:0 or 16:0 lyso-PC in MOPS buffer and vortexing for 1 min. Stocks were diluted to a working lipid concentration of 25 mM. Vesicles and micelles were used immediately after preparation, and all buffers were filtered through a 0.22-μm membrane (Millipore).

Dynamic light scattering (DLS)

Light scattering was measured at 20 °C based on prior methods using Dynapro NanoStar (Wyatt Technology) (19). Autoattenuation of the laser power maintained the intensity at ~1.0 to 2.5 × 10^6 counts/s, and 10 5-s acquisitions were collected. Using the regularization fit and Rayleigh sphere model, the average hydrodynamic radius was estimated using Dynamics Version 7.0.2 software. Vesicle size was determined immediately after production.

Phosphorous quantification assay

Lipid concentration was determined using a colorimetric assay (68) modified from Avanti Polar Lipids. Absorbance at 820 nm was measured on a Cary 300 Bio spectrophotometer (2.0 s average time, 1.5-nm bandwidth). A standardization curve was made daily using a sodium phosphate dibasic standard (1000 ± 4 mg/liter).

Differential scanning calorimetry (DSC)

Thermograms were obtained using a Microcal VP-DSC calorimeter (Malvern Instruments). Buffer and lipid samples (700 μl) were de-gassed for 10 min at 20 °C before injection into the calorimeter. Prior to measurements, samples were equilibrated at 20 °C for 20 min. Then, two scans were taken where the temperature was increased at a scan rate of 20 °C/h. Final graphs were obtained by subtracting the buffer thermogram from the sample scan. Data analysis involved normalization to

the lipid concentration and subtraction of the baseline. T_m was extracted from fitting the data to a two-state model (Origin 7).

CD spectroscopy

Protein samples were exchanged into buffer (20 mM MOPS, 100 mM NaCl, pH 7) using a PD-10 column (GE Healthcare) and allowed to equilibrate for 10 min at room temperature with the SUVs. CD spectra were collected in 1-mm quartz cuvettes using a Jasco J-715 spectropolarimeter (Jasco Analytical Instruments) with the following settings: 200–260 nm, continuous mode, 100 nm/min scan rate, 1 nm bandwidth, 1 nm steps, and three accumulations at 20 °C. To improve signal-to-noise for some of the samples (DOPC and DOPC/SM/Chol), CD signals at 222 nm were averaged over 1 min at 20 °C. Binding curves were generated from mean residue ellipticity ([θ]) and fit to a two-state equilibrium where α-syn partitions between the vesicle and the solution, as described previously (19), using Igor Pro 6.37 (WaveMetrics). In addition, temperature scans were performed by first incubating the sample at the starting temperature for 10 min. Then, data were collected at 222 nm using the following settings: 20 °C/h scan rate, 1 nm bandwidth, and 0.2 °C steps.

Isothermal calorimetry (ITC)

A Microcal iTC200 (Malvern Instruments) equipped with a motor-driven syringe was used to titrate DPPC SUVs (45 mM) into a given protein sample (2 μM) equilibrated at either 20 or 50 °C. The cell containing the protein was ~200 μl, and 20 injections of 2 μl each were performed. Data analysis, including integration of the raw isotherms and normalization to the protein and lipid concentrations, was performed using NITPIC (version 1.2.2) and MicroCal ORIGIN software.

Aggregation kinetics

N-Acetyl α-syn was exchanged into buffer (20 mM MOPS, 100 mM NaCl, pH 7) using a PD-10 column (GE Healthcare) and filtered through a YM-100 centrifugal filter unit (Millipore) to remove pre-formed aggregates. Aggregation was performed in a 384-well flat bottom plate (Greiner Bio-One, catalog no. 781209) sealed with an adhesive film (ThermoFisher Scientific, catalog no. 4311971) using a Tecan Spark microplate reader at 37 °C with continuous linear shaking (1 mm) for ~4–5 days. Each well contained one 2-mm glass bead and 80 μl of sample (50 μM N-acetyl α-syn and 10 μM ThT) in the presence (50 μM to 5 mM) or absence of lipid vesicles as specified. Buffer and lipid alone controls were also measured. ThT fluorescence was excited at 415 nm and detected at 480 nm (top read, 25 flashes, and a gain setting of 90).

TEM

Samples were evaluated before and after aggregation according to previously described procedures (19). Samples (3 μl) were applied for 1–2 min to TEM grids (400-mesh Formvar and carbon-coated copper, Electron Microscopy Sciences) that were glow-discharged for 1 min at 0.26 mbar (PELCO easiGlow). Sample was wicked with filter paper, washed with water (3 μl), and stained with three drops of 1% (w/v) aqueous uranyl acetate solution. The stain was immediately wicked away, and the grid was left to air dry. TEM was performed using either a JEOL JEM 1200EXII transmission electron microscope (accelerating voltage 80 keV) equipped with an AMT XR-60 digital camera or a JEOL JEM1400 transmission electron microscope (accelerating voltage 120 keV) with an AMT XR-111 digital camera.

Author contributions—E. I. O. made proteins, collected and analyzed data, and wrote the paper; Z. J. made proteins and designed experiments; M.-P. S. made the β- and γ-syn constructs; J. C. L. conceived the study and wrote the paper with E. I. O.

Acknowledgments—Parts of this research were performed on instruments maintained by the NHLBI Biophysics (CD, DSC, DLS, and ITC), Biochemistry (LC-MS), and Electron Microscopy (TEM) Core Facilities. We thank Dan Mulvihill (University of Kent) for the gift of the pNatB plasmid and Di Wu (NHLBI Biophysics Core Facility, National Institutes of Health) in aiding with the ITC data analysis.

References

1. Dorsey, E. R., Constantinescu, R., Thompson, J. P., Biglan, K. M., Holloway, R. G., Kieburtz, K., Marshall, F. J., Ravina, B. M., Schifitto, G., Siderowf, A., and Tanner, C. M. (2007) Projected number of people with Parkinson disease in the most populous nations, 2005 through 2030. *Neurology* **68,** 384–386 CrossRef Medline
2. Spillantini, M. G., Schmidt, M. L., Lee, V. M., Trojanowski, J. Q., Jakes, R., and Goedert, M. (1997) α-Synuclein in Lewy bodies. *Nature* **388,** 839–840 CrossRef Medline
3. Xu, L. J., and Pu, J. L. (2016) α-Synuclein in Parkinson's disease: from pathogenetic dysfunction to potential clinical application. *Parkinsons Dis. 2016,* 1720621 CrossRef Medline
4. Maroteaux, L., Campanelli, J. T., and Scheller, R. H. (1988) Synuclein–a neuron-specific protein localized to the nucleus and presynaptic nerve-terminal. *J. Neurosci.* **8,** 2804–2815 CrossRef Medline
5. Vargas, K. J., Schrod, N., Davis, T., Fernandez-Busnadiego, R., Taguchi, Y. V., Laugks, U., Lucic, V., and Chandra, S. S. (2017) Synucleins have multiple effects on presynaptic architecture. *Cell Rep.* **18,** 161–173 CrossRef Medline
6. Perez, R. G., and Hastings, T. G. (2004) Could a loss of α-synuclein function put dopaminergic neurons at risk? *J. Neurochem.* **89,** 1318–1324 CrossRef Medline
7. Fujita, Y., Ohama, E., Takatama, M., Al-Sarraj, S., and Okamoto, K. (2006) Fragmentation of Golgi apparatus of nigral neurons with α-synuclein-positive inclusions in patients with Parkinson's disease. *Acta Neuropathol.* **112,** 261–265 CrossRef Medline
8. Meredith, G. E., Totterdell, S., Petroske, E., Santa Cruz, K., Callison, R. C., Jr., and Lau, Y. S. (2002) Lysosomal malfunction accompanies α-synuclein aggregation in a progressive mouse model of Parkinson's disease. *Brain Res.* **956,** 156–165 CrossRef Medline
9. Nakamura, K., Nemani, V. M., Azarbal, F., Skibinski, G., Levy, J. M., Egami, K., Munishkina, L., Zhang, J., Gardner, B., Wakabayashi, J., Sesaki, H., Cheng, Y., Finkbeiner, S., Nussbaum, R. L., Masliah, E., and Edwards, R. H. (2011) Direct membrane association drives mitochondrial fission by the Parkinson disease-associated protein α-synuclein. *J. Biol. Chem.* **286,** 20710–20726 CrossRef Medline
10. Beyer, K. (2007) Mechanistic aspects of Parkinson's disease: α-Synuclein and the biomembrane. *Cell Biochem. Biophys.* **47,** 285–299 CrossRef Medline
11. Butterfield, S. M., and Lashuel, H. A. (2010) Amyloidogenic protein membrane interactions: mechanistic insight from model systems. *Angew. Chem. Int. Ed. Engl.* **49,** 5628–5654 CrossRef Medline
12. Pfefferkorn, C. M., Jiang, Z., and Lee, J. C. (2012) Biophysics of α-synuclein membrane interactions. *Biochim. Biophys. Acta* **1818,** 162–171 CrossRef Medline

13. Georgieva, E. R., Ramlall, T. F., Borbat, P. P., Freed, J. H., and Eliezer, D. (2010) The lipid-binding domain of wild type and mutant α-synuclein compactness and interconversion between the broken and extended helix forms. *J. Biol. Chem.* **285,** 28261–28274 CrossRef Medline
14. Bartels, T., Ahlstrom, L. S., Leftin, A., Kamp, F., Haass, C., Brown, M. F., and Beyer, K. (2010) The N terminus of the intrinsically disordered protein α-synuclein triggers membrane binding and helix folding. *Biophys. J.* **99,** 2116–2124 CrossRef Medline
15. Davidson, W. S., Jonas, A., Clayton, D. F., and George, J. M. (1998) Stabilization of α-synuclein secondary structure upon binding to synthetic membranes. *J. Biol. Chem.* **273,** 9443–9449 CrossRef Medline
16. Eliezer, D., Kutluay, E., Bussell, R., Jr., and Browne, G. (2001) Conformational properties of α-synuclein in its free and lipid-associated states. *J. Mol. Biol.* **307,** 1061–1073 CrossRef Medline
17. Jiang, Z., de Messieres, M., and Lee, J. C. (2013) Membrane remodeling by α-synuclein and effects on amyloid formation. *J. Am. Chem. Soc.* **135,** 15970–15973 CrossRef Medline
18. Jiang, Z., Heinrich, F., McGlinchey, R. P., Gruschus, J. M., and Lee, J. C. (2017) Segmental deuteration of α-synuclein for neutron reflectometry on tethered bilayers. *J. Phys. Chem. Lett.* **8,** 29–34 CrossRef Medline
19. Jiang, Z., Hess, S. K., Heinrich, F., and Lee, J. C. (2015) Molecular details of α-synuclein membrane association revealed by neutrons and photons. *J. Phys. Chem. B* **119,** 4812–4823 CrossRef Medline
20. Pfefferkorn, C. M., Heinrich, F., Sodt, A. J., Maltsev, A. S., Pastor, R. W., and Lee, J. C. (2012) Depth of α-synuclein in a bilayer determined by fluorescence, neutron reflectometry, and computation. *Biophys. J.* **102,** 613–621 CrossRef Medline
21. Pfefferkorn, C. M., and Lee, J. C. (2010) Tryptophan probes at the α-synuclein and membrane interface. *J. Phys. Chem. B* **114,** 4615–4622 CrossRef Medline
22. Yap, T. L., Jiang, Z., Heinrich, F., Gruschus, J. M., Pfefferkorn, C. M., Barros, M., Curtis, J. E., Sidransky, E., and Lee, J. C. (2015) Structural features of membrane-bound glucocerebrosidase and α-synuclein probed by neutron reflectometry and fluorescence spectroscopy. *J. Biol. Chem.* **290,** 744–754 CrossRef Medline
23. Chong, S. S., Taneva, S. G., Lee, J. M., and Cornell, R. B. (2014) The curvature sensitivity of a membrane-binding amphipathic helix can be modulated by the charge on a flanking region. *Biochemistry* **53,** 450–461 CrossRef Medline
24. Kjaer, L., Giehm, L., Heimburg, T., and Otzen, D. (2009) The influence of vesicle size and composition on α-synuclein structure and stability. *Biophys. J.* **96,** 2857–2870 CrossRef Medline
25. Jo, E., McLaurin, J., Yip, C. M., St George-Hyslop, P., and Fraser, P. E. (2000) α-Synuclein membrane interactions and lipid specificity. *J. Biol. Chem.* **275,** 34328–34334 CrossRef Medline
26. Middleton, E. R., and Rhoades, E. (2010) Effects of curvature and composition on α-synuclein binding to lipid vesicles. *Biophys. J.* **99,** 2279–2288 CrossRef Medline
27. Ramakrishnan, M., Jensen, P. H., and Marsh, D. (2003) α-Synuclein association with phosphatidylglycerol probed by lipid spin labels. *Biochemistry* **42,** 12919–12926 CrossRef Medline
28. Nuscher, B., Kamp, F., Mehnert, T., Odoy, S., Haass, C., Kahle, P. J., and Beyer, K. (2004) α-Synuclein has a high affinity for packing defects in a bilayer membrane–a thermodynamics study. *J. Biol. Chem.* **279,** 21966–21975 CrossRef Medline
29. Kamp, F., and Beyer, K. (2006) Binding of α-synuclein affects the lipid packing in bilayers of small vesicles. *J. Biol. Chem.* **281,** 9251–9259 CrossRef Medline
30. Pirc, K., and Ulrih, N. P. (2015) α-Synuclein interactions with phospholipid model membranes: key roles for electrostatic interactions and lipid-bilayer structure. *Biochim. Biophys. Acta* **1848,** 2002–2012 CrossRef Medline
31. Stöckl, M., Fischer, P., Wanker, E., and Herrmann, A. (2008) α-Synuclein selectively binds to anionic phospholipids embedded in liquid-disordered domains. *J. Mol. Biol.* **375,** 1394–1404 CrossRef Medline
32. Levi, M., Wilson, P., Nguyen, S., Iorio, E., Sapora, O., and Parasassi, T. (1997) In K562 and HL60 cells membrane ageing during cell growth is associated with changes in cholesterol concentration. *Mech. Ageing Dev.* **97,** 109–119 CrossRef Medline
33. Fabelo, N., Martín, V., Santpere, G., Marín, R., Torrent, L., Ferrer, I., and Díaz, M. (2011) Severe alterations in lipid composition of frontal cortex lipid rafts from Parkinson's disease and incidental Parkinson's disease. *Mol. Med.* **17,** 1107–1118 Medline
34. Giusto, N. M., Salvador, G. A., Castagnet, P. I., Pasquaré, S. J., and Ilincheta de Boschero, M. G. I. (2002) Age-associated changes in central nervous system glycerolipid composition and metabolism. *Neurochem. Res.* **27,** 1513–1523 CrossRef Medline
35. Kranenburg, M., and Smit, B. (2005) Phase behavior of model lipid bilayers. *J. Phys. Chem. B* **109,** 6553–6563 CrossRef Medline
36. Quinn, P. J., and Wolf, C. (2009) The liquid-ordered phase in membranes. *Biochim. Biophys. Acta* **1788,** 33–46 CrossRef Medline
37. Rietveld, A., and Simons, K. (1998) The differential miscibility of lipids as the basis for the formation of functional membrane rafts. *Biochim. Biophys. Acta* **1376,** 467–479 CrossRef Medline
38. Kubo, S., Nemani, V. M., Chalkley, R. J., Anthony, M. D., Hattori, N., Mizuno, Y., Edwards, R. H., and Fortin, D. L. (2005) A combinatorial code for the interaction of α-synuclein with membranes. *J. Biol. Chem.* **280,** 31664–31672 CrossRef Medline
39. Rhoades, E., Ramlall, T. F., Webb, W. W., and Eliezer, D. (2006) Quantification of α-synuclein binding to lipid vesicles using fluorescence correlation spectroscopy. *Biophys. J.* **90,** 4692–4700 CrossRef Medline
40. Leftin, A., Job, C., Beyer, K., and Brown, M. F. (2013) Solid-state C-13 NMR reveals annealing of raft-like membranes containing cholesterol by the intrinsically disordered protein α-synuclein. *J. Mol. Biol.* **425,** 2973–2987 CrossRef Medline
41. Arnesen, T., Van Damme, P., Polevoda, B., Helsens, K., Evjenth, R., Colaert, N., Varhaug, J. E., Vandekerckhove, J., Lillehaug, J. R., Sherman, F., and Gevaert, K. (2009) Proteomics analyzes reveal the evolutionary conservation and divergence of N-terminal acetyltransferases from yeast and humans. *Proc. Natl. Acad. Sci. U.S.A.* **106,** 8157–8162 CrossRef Medline
42. Anderson, J. P., Walker, D. E., Goldstein, J. M., de Laat, R., Banducci, K., Caccavello, R. J., Barbour, R., Huang, J., Kling, K., Lee, M., Diep, L., Keim, P. S., Shen, X., Chataway, T., Schlossmacher, M. G., *et al.* (2006) Phosphorylation of Ser-129 is the dominant pathological modification of α-synuclein in familial and sporadic Lewy body disease. *J. Biol. Chem.* **281,** 29739–29752 CrossRef Medline
43. Ohrfelt, A., Zetterberg, H., Andersson, K., Persson, R., Secic, D., Brinkmalm, G., Wallin, A., Mulugeta, E., Francis, P. T., Vanmechelen, E., Aarsland, D., Ballard, C., Blennow, K., and Westman-Brinkmalm, A. (2011) Identification of novel α-synuclein isoforms in human brain tissue by using an online NanoLC-ESI-FTICR-MS method. *Neurochem. Res.* **36,** 2029–2042 CrossRef Medline
44. Zabrocki, P., Bastiaens, I., Delay, C., Barmmens, T., Ghillebert, R., Pellens, K., De Virgilio, C., Van Leuven, F., and Winderickx, J. (2008) Phosphorylation, lipid raft interaction and traffic of α-synuclein in a yeast model for Parkinson. *Biochim. Biophys. Acta* **1783,** 1767–1780 CrossRef Medline
45. Dikiy, I., and Eliezer, D. (2014) N-terminal acetylation stabilizes N-terminal helicity in lipid- and micelle-bound α-synuclein and increases its affinity for physiological membranes. *J. Biol. Chem.* **289,** 3652–3665 CrossRef Medline
46. Maltsev, A. S., Ying, J., and Bax, A. (2012) Impact of N-terminal acetylation of α-synuclein on its random coil and lipid binding properties. *Biochemistry* **51,** 5004–5013 CrossRef Medline
47. Fauvet, B., Fares, M. B., Samuel, F., Dikiy, I., Tandon, A., Eliezer, D., and Lashuel, H. A. (2012) Characterization of semisynthetic and naturally N^{α}-acetylated α-synuclein *in vitro* and in intact cells implications for aggregation and cellular properties of α-synuclein. *J. Biol. Chem.* **287,** 28243–28262 CrossRef Medline
48. Jao, C. C., Hegde, B. G., Chen, J., Haworth, I. S., and Langen, R. (2008) Structure of membrane-bound α-synuclein from site-directed spin labeling and computational refinement. *Proc. Natl. Acad. Sci. U.S.A.* **105,** 19666–19671 CrossRef Medline
49. Stafford, R. E., Fanni, T., and Dennis, E. A. (1989) Interfacial properties and critical micelle concentration of lysophospholipids. *Biochemistry* **28,** 5113–5120 CrossRef Medline

50. Vanni, S., Hirose, H., Barelli, H., Antonny, B., and Gautier, R. (2014) A sub-nanometre view of how membrane curvature and composition modulate lipid packing and protein recruitment. *Nat. Commun.* **5,** 4916 CrossRef Medline
51. Cui, H., Lyman, E., and Voth, G. A. (2011) Mechanism of membrane curvature sensing by amphipathic helix containing proteins. *Biophys. J.* **100,** 1271–1279 CrossRef Medline
52. Veatch, S. L., and Keller, S. L. (2005) Seeing spots: complex phase behavior in simple membranes. *Biochim. Biophys. Acta* **1746,** 172–185 CrossRef Medline
53. Ulmer, T. S., Bax, A., Cole, N. B., and Nussbaum, R. L. (2005) Structure and dynamics of micelle-bound human α-synuclein. *J. Biol. Chem.* **280,** 9595–9603 CrossRef Medline
54. Leonenko, Z. V., Finot, E., Ma, H., Dahms, T. E., and Cramb, D. T. (2004) Investigation of temperature-induced phase transitions in DOPC and DPPC phospholipid bilayers using temperature-controlled scanning force microscopy. *Biophys. J.* **86,** 3783–3793 CrossRef Medline
55. Chernomordik, L. V., and Kozlov, M. M. (2003) Protein-lipid interplay in fusion and fission of biological membranes. *Annu. Rev. Biochem.* **72,** 175–207 CrossRef Medline
56. Burré, J., Sharma, M., and Südhof, T. C. (2014) α-Synuclein assembles into higher-order multimers upon membrane binding to promote SNARE complex formation. *Proc. Natl. Acad. Sci. U.S.A.* **111,** E4274–E4283 CrossRef Medline
57. Burré, J., Sharma, M., Tsetsenis, T., Buchman, V., Etherton, M. R., and Südhof, T. C. (2010) α-Synuclein promotes SNARE-complex assembly *in vivo* and *in vitro*. *Science* **329,** 1663–1667 CrossRef Medline
58. Rizo, J., and Südhof, T. C. (2002) SNAREs and Munc18 in synaptic vesicle fusion. *Nat. Rev. Neurosci.* **3,** 641–653 CrossRef Medline
59. Fortin, D. L., Troyer, M. D., Nakamura, K., Kubo, S., Anthony, M. D., and Edwards, R. H. (2004) Lipid rafts mediate the synaptic localization of α-synuclein. *J. Neurosci.* **24,** 6715–6723 CrossRef Medline
60. Chartier-Harlin, M. C., Kachergus, J., Roumier, C., Mouroux, V., Douay, X., Lincoln, S., Levecque, C., Larvor, L., Andrieux, J., Hulihan, M., Waucquier, N., Defebvre, L., Amouyel, P., Farrer, M., and Destée, A. (2004) α-Synuclein locus duplication as a cause of familial Parkinson's disease. *Lancet* **364,** 1167–1169 CrossRef Medline
61. Singleton, A. B., Farrer, M., Johnson, J., Singleton, A., Hague, S., Kachergus, J., Hulihan, M., Peuralinna, T., Dutra, A., Nussbaum, R., Lincoln, S., Crawley, A., Hanson, M., Maraganore, D., Adler, C., *et al.* (2003) α-Synuclein locus triplication causes Parkinson's disease. *Science* **302,** 841–841 CrossRef Medline
62. Chiba-Falek, O., Lopez, G. J., and Nussbaum, R. L. (2006) Levels of α-synuclein mRNA in sporadic Parkinson disease patients. *Mov. Disord.* **21,** 1703–1708 CrossRef Medline
63. Xilouri, M., Brekk, O. R., and Stefanis, L. (2013) α-Synuclein and protein degradation systems: a reciprocal relationship. *Mol. Neurobiol.* **47,** 537–551 CrossRef Medline
64. Galvagnion, C. (2017) The role of lipids interacting with α-synuclein in the pathogenesis of Parkinson's disease. *J. Parkinson Dis.* **7,** 433–450 CrossRef Medline
65. McGlinchey, R. P., Dominah, G. A., and Lee, J. C. (2017) Taking a bite out of amyloid: mechanistic insights into α-synuclein degradation by cathepsin L. *Biochemistry* **56,** 3881–3884 CrossRef Medline
66. Jakes, R., Spillantini, M. G., and Goedert, M. (1994) Identification of 2 distinct synucleins from human brain. *FEBS Lett.* **345,** 27–32 CrossRef Medline
67. Johnson, M., Coulton, A. T., Geeves, M. A., and Mulvihill, D. P. (2010) Targeted amino-terminal acetylation of recombinant proteins in *E. coli*. *PLoS One* **5,** e15801 CrossRef Medline
68. Brisbois, C. A., and Lee, J. C. (2016) Apolipoprotein C-III nanodiscs studied by site-specific tryptophan fluorescence. *Biochemistry* **55,** 4939–4948 CrossRef Medline